Calibration of the SMAP Soil Moisture Retrieval Algorithm to Reduce Bias Over the Amazon Rainforest

Kyeungwoo Cho, Robinson Negrón-Juárez, Andreas Colliander, *Senior Member, IEEE*, Eric G. Cosio, Norma Salinas, Alessandro de Araujo, Jefferey Q. Chambers, and Jingfeng Wang

***Abstract*—Soil moisture (*SM*) is crucial for the Earth's ecosystem, impacting climate and vegetation health. Obtaining in situ observations of *SM* is labor-intensive and complex, particularly in remote and densely vegetated regions like the Amazon rainforest. NASA's soil moisture active and passive (SMAP) mission, utilizing an L-band radiometer, aims to monitor global *SM*. While it has been validated in areas with low vegetation water content (*VWC*) (< 5 kgm^{-2}), its efficiency in the Amazon, with dense canopies and high *VWC* (> 10 kgm^{-2}), is limitedly investigated due to scarce in situ measurements. This study assessed and analyzed the SMAP *SM* retrievals in the Amazon, employing the single-channel algorithm and adjusting vegetation optical depth (τ) and single scattering albedo (ω), two key vegetation parameters. It incorporated in situ *SM* observations from three old-growth rainforest locations: Tambopata (Southwest Amazon), Manaus (Central Amazon), and Caxiuana (Eastern Amazon). The SMAP *SM* deviated substantially from the in situ *SM*. However, calibrating τ and ω values, characterized by a lower τ, resulted in better agreement with the in situ measurements. This study emphasizes the pressing need for innovative methodologies to accurately retrieve *SM* in high-*VWC* regions like the Amazon rainforest using SMAP data.**

***Index Terms*—Amazon rainforest, remote sensing, soil moisture (*SM*), soil moisture active/passive (SMAP), vegetation optical depth (*VOD*).**

Manuscript received 20 January 2024; revised 19 March 2024; accepted 10 April 2024. Date of publication 15 April 2024; date of current version 29 April 2024. This work was supported by NASA SMAP Science Team Funding under Grant 80HQTR21T0064. The Manaus soil moisture data is funded by the Next Generation Ecosystem Experiments-Tropics, which is funded by the U.S. Department of Energy, Office of Science, Office of Biological and Environmental Research. The work of Robinson Negrón-Juárez was supported in part by this initiative. The Tambopata site is funded by CONCYTEC-World Bank 057-2018-FONDECYT-BM-IADT-MU and CONCYTEC-World Bank under Grant 011-2019-FONDECYT-BM-INC-INV. Contributions to this work were also made at the Jet Propulsion Laboratory, California Institute of Technology, operating under a contract with the National Aeronautics and Space Administration. *(Corresponding author: Kyeungwoo Cho.)*

Kyeungwoo Cho and Jingfeng Wang are with the Georgia Institute of Technology, Atlanta, GA 30332 USA (e-mail: kyeungwoo.cho@gatech.edu; jingfeng.wang@ce.gatech.edu).

Robinson Negrón-Juárez and Jefferey Q. Chambers are with the Lawrence Berkeley National Laboratory, Climate and Ecosystem Sciences Division, Berkeley, CA 94705 USA (e-mail: robinson.inj@lbl.gov; jqchambers@berkeley.edu).

Andreas Colliander is with the Jet Propulsion Laboratory, California Institute of Technology, Pasadena, CA 91125 USA (e-mail: andreas.colliander@jpl.nasa.gov).

Eric G. Cosio and Norma Salinas are with the Chemistry Section, Pontifical Catholic University of Peru, Lima 15088, Peru (e-mail: ecosio@pucp.pe; nsalinasr@pucp.pe).

Alessandro de Araujo is with the Embrapa Amazonia Oriental, Belém 66095-903, Brazil (e-mail: alessandro.araujo@embrapa.br).

Digital Object Identifier 10.1109/JSTARS.2024.3388914

I. Introduction

Soil moisture *(SM)* is a key component of water and energy cycles [1], [2], [3], [4] affecting evapotranspiration, infiltration, and runoff [1], [2], [5]. *SM* is also a vital source of water, supporting ecosystem function, and productivity [6], [7]. Precise estimation and consistent monitoring of *SM* are paramount to comprehending climate change and its subsequent ramifications on the ecosystem, particularly during extended periods of drought [8], [9].

In situ observations of *SM* are significantly laborious and have the capacity to offer observations on a comparatively small scale [10]. In remote areas these measurements are scarce. To overcome these limitations, satellite observations of *SM* have been devised as a compelling alternative. Satellites, utilizing optical, thermal, and microwave signals, are proficient in ceaselessly observing the spatial distributions of *SM* [11].

The soil moisture active and passive (SMAP) mission [12] is focused on measuring global *SM* through the employment of an L-band (1.41 GHz) microwave radiometer. The National Aeronautics and Space Administration (NASA) launched the SMAP satellite in January 2015, its primary goal being the observation of global *SM* and the freeze-thaw state of soil, utilizing both active and passive microwave sensors. However, after the malfunction of the active sensor, since July 2015, SMAP has been reliant solely on its passive sensor for the collection of *SM* data. Passive microwave remote sensing at low frequency can provide global *SM* at a high temporal resolution, with minimal interference from weather conditions and surface roughness. SMAP provides *SM* data retrieved through algorithms predicated on the correlation between the soil dielectric constant and *SM* [13], [14], [15]. SMAP *SM* retrieval algorithms include the single-channel algorithm (SCA) and the dual-channel algorithm (DCA). These algorithms utilize vertically polarized brightness temperature (T_{BV}) and horizontally polarized brightness temperatures (T_{BH}) as their input parameters. The suite of available SMAP products includes Level-2 (half-orbit, with a resolution of 36 km) and Level-3 (daily composite, with a resolution of

36 km), both capturing the top 5 cm depth of *SM*. Each level of data also includes enhanced products, providing improved quality and a more granular 9 km spatial resolution. The SMAP Level-2 and Level-3 *SM* data products incorporate *SM* data retrieved from both the T_{BV}-based single-channel algorithm (SCA-V), the T_{BH}-based single-channel algorithm (SCA-H), and the DCA. DCA has emerged as the standard baseline algorithm for SMAP [16].

The accuracy of the SMAP *SM* products has been validated against field observations at sites comprising a variety of land cover types. Colliander et al. [17] assessed the performance of the SMAP *SM* products using data collected from 18 core validation sites. The results confirmed that SMAP radiometer-based *SM* data products exhibit high fidelity (with an unbiased root mean squared difference (ubRMSD) less than $0.04\ \mathrm{m^3m^{-3}}$) in areas with a vegetation water content (*VWC*) below $5\ \mathrm{kgm^{-2}}$. Ayres et al. [18] conducted SMAP *SM* data validation against the in situ *SM* observations collected from 40 National Ecological Observatory Network sites, including 19 forest locations. The SMAP *SM* data were reliable over unforested regions (ubRMSD $0.046\ \mathrm{m^3m^{-3}}$; the spatial representativeness errors inflate the ubRMSD values compared with the core sites), while the SMAP *SM* data over forested regions were less accurate (ubRMSD 0.053–0.060 $\mathrm{m^3m^{-3}}$). Other validation studies emphasized reconsidering physical temperature, vegetation transmission, and scattering parameters in *SM* retrieval for forest-covered regions [19]. The SMAP *SM* data overall has been confirmed to possess commendable quality for nonforested regions, but it requires further enhancements for densely forested regions with *VWC* within the range of 6–18 $\mathrm{kgm^{-2}}$ (e.g., [20]). Notably, the Amazon rainforest, with its high and dense tree coverage [21], [22], has a *VWC* approximately $15\ \mathrm{kgm^{-2}}$ [23].

Efforts to improve *SM* retrieval have been numerous and noteworthy. For instance, Konings et al. [24] introduced the multitemporal DCA (MT-DCA), retrieving *SM*, vegetation optical depth (*VOD*), and effective scattering albedo. The MT-DCA led to a reduction in ubRMSD ($\sim$0.01 $\mathrm{m^3m^{-3}}$) of *SM* retrievals when compared with the SCA-V, barring tropical forests and agriculture regions. The authors in [25] and [26] further refined the DCA implementation for the SMAP *SM* product, outperforming SCA-V [17]. Recently, Li et al. [27] introduced SMAP-INRAE-BORDEAUX (SMAP-IB), built on the L-band microwave emission of the biosphere model. Their findings suggest that SMAP-IB can simulate global *SM* with similar performance to SCA-V and better performance than MT-DCA and DCA at 36 km resolution. However, the performance of SMAP-IB appears to be similar to, or less satisfactory than, that of SCA-V in areas covered with shrublands, woody savannas, croplands, and cropland/natural mosaics [27]. More efforts are made to use multiple channels and frequency measurements to improve the robustness of *SM* retrieval [28].

The diminished performance of SMAP in areas of dense vegetation can be ascribed to an inadequate accounting of the vegetation cover interference in microwave remote sensing. Mitigating this issue necessitates precise estimation of the impact of vegetation on microwave-based remote sensing, which in turn calls for accurate determination of radiative transfer model variables such as *VWC* and *VOD* [24], [29]. The SMAP SCA employs *VWC* derived from normalized difference vegetation index (NDVI). This approach, while pragmatic, does not capture the interannual variability in vegetation seasonality and is susceptible to saturation [23]. The calculated *VWC* is used to determine the *VOD* by applying a constant parameter. In contrast to the SCA, SMAP DCA estimates *VOD* by utilizing measurements from both T_{BV} and T_{BH}. However, it is acknowledged that minimization of the variance between the brightness temperatures (T_B) in vertical and horizontal polarization can limit the effectiveness of the DCA for accurately simulating *VOD* [30], [31]. While several studies have endeavored to assess and improve *VOD* [24], [26], as well as assess *SM* in tropical regions [32], the lack of in situ *VWC* and *VOD* data makes it difficult to evaluate their accuracy.

The Amazon rainforest, the world's largest tropical rainforest, represents 60% of the global tropical forest. These forests play a crucial role in the global water cycle, transpiring massive amounts of water [33], and accounting for nearly 50% of the region's rainfall via evapotranspiration [12], [34]. Despite the critical role of *SM* in understanding evapotranspiration over the Amazon rainforest [35], [36], [37], logistical difficulties have led to a scarcity of in situ *SM* observations. The dense and tall canopy cover of the Amazon rainforest further complicates microwave remote sensing of *SM*. Microwaves emanating from the soil surface undergo modulation due to attenuation and scattering within the canopy layer [38]. This interference in the canopy layer significantly affects the clarity and accuracy of the signals received from the soil, complicating the measurement of *SM*. To date, SMAP *SM* data over the Amazon rainforest has not been thoroughly analyzed. As the first-ever study comparing in situ observations of *SM* in the Amazon and SMAP *SM*, our objective is to evaluate the accuracy and performance of the SMAP Level-3 Enhanced *SM* product by optimizing the parameters of the SMAP SCA-V algorithm for areas with dense canopy cover.

II. Material and Methods

A. Study Sites

The three sites selected for this study are located within various climatic zones of the Amazon rainforest (Fig. 1), characterized by dense, old-growth trees that reach heights up to 30 m. The first site, Tambopata (12.831° S, 69.283° W), is located within the Tambopata National Forests of Peru, adjacent to the Tambopata River. This region undergoes a dry season spanning 4 to 5 months, commencing in May, with an annual mean temperature of 26°C and a mean annual rainfall (MAR) that fluctuates between 1600 and 2400 mm. Lopez-Gonzalez et al. [39] report a tree density of 556 trees per hectare in this area, with a basal area of 25.9 square meters per hectare. Data from in situ *SM* measurements have been available from this site on a half-hourly basis since November 2020, utilizing an *SM* sensor that is installed at a depth of 5 cm within the soil layer. In 2022, this profile was extended to a depth of 1 m, starting at 5 cm depth. The second site, Manaus (2.609° S, 60.209° W), is located approximately 53 km north of the city of Manaus in Amazonas State, Brazil. This area endures a dry

Fig. 1. Study sites in the Amazon rainforest (yellow dots). The green line denotes the boundary of the Amazon rainforest. The figure was generated by ArcGIS Pro version 3.0.0.

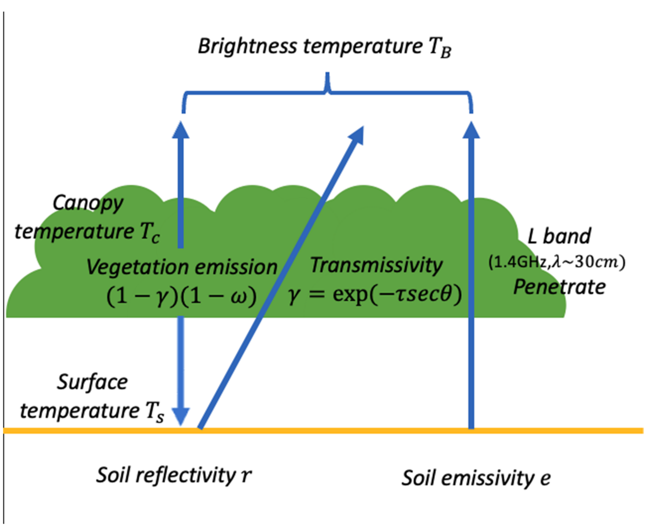

Fig. 2. Diagram of the $\tau-\omega$ model with canopy layer (illustrated in green). The brightness temperature ($\boldsymbol{T_B}$) is represented as the summation of the radiative energy originating from the soil surface (depicted by the yellow line) and the contribution modified by the overlaying canopy layer.

season lasting 3 months, typically starting in July, with an annual mean temperature similar to Tambopata at 26°C and MAR is 2200 mm. The basal area of Manaus is 29 square meters per hectare [40]. Half-hourly *SM* data for the Manaus site have been accessible since September 2018 [37]. *SM* sensors are installed at 13 different depths ranging from 0.025 to 14.3 m. The third site, Caxiuana (1.708° S, 51.529° W), is situated within the Caxiuana National Forest, approximately 350 km west of the city of Belem in Para State, Brazil. The Caxiuana site experiences a dry season lasting 4 months, typically commencing in August, with a MAR of 2000 mm. The aboveground dry biomass in this

TABLE I
Summary of In-Situ Observations of SM in Amazon Sites

Site	Location	Measurement depth (m) (*depth used as surface SM)	Available period
Manaus	2.609°S, 60.209°W	0.025* - 14.3	2018/09/01–2020/01/31
Tambopata	12.831°S, 69.283°W	0.05*	2020/10/19–2021/09/15
Caxiuana	1.708°S, 51.529°W	0.2* - 1	2018/05/28–2021/01/01

area is estimated to be around 200 cubic meters per hectare, while the basal area varies between 30 and 35 square meters per hectare [40]. At this site, half-hourly *SM* data have been recorded at multiple depths ranging from 20 to 100 cm since 2016. These three sites are dispersed throughout the central, southeastern, and western regions (Fig. 1). In this study, we utilized the shallowest observation depth at each site and the corresponding available data period as presented in Table I. The in situ datasets utilized in this study are not publicly available at this time as they have not yet been published.

B. SMAP Level-3 Enhanced Product

The SMAP Level-3 Enhanced product (SPL3SMP_E, version 5), integral to this study, can be obtained from the National Snow and Ice Data Center [41]. The SMAP satellite operates with a 40° incident angle from the nadir and traverses the equator at local solar time (LST) 6 AM (descending) and 6 PM (ascending), thus enveloping the globe every 2–3 days. The SMAP Level-3 Enhanced product has a spatial resolution of 33 km, which is projected onto a 9 km by 9 km equal-area scalable Earth-2 (EASE2) grid [42]. The SMAP L-band radiometer measures antenna temperature, which subsequently gets converted to T_B and gridded on the EASE2 grid using the Backus–Gilbert optimal interpolation technique. The SMAP Level-3 Enhanced product is essentially a daily composite of the SMAP Level-2 *SM* product. In addition to providing DCA and SCA *SM* retrievals from both T_{BV} and T_{BH}, the SMAP Level-3 Enhanced product also furnishes ancillary data, including the NASA Goddard Modeling Assimilation Office GEOS-FP model effective surface temperature [16].

For this study, T_B measured at 6 AM LST was used, which is the primary overpass time typically employed in the validation of SMAP *SM* products [17]. This time was specifically chosen because the thermal gradient of the soil-vegetation continuum is generally smaller at 6 AM than at 6 PM [43]. The T_{BV}-based *SM* retrievals exhibit a higher quality than their T_{BH} counterparts [17], [44]. Consequently, this study leveraged only T_{BV} and *SM* retrieved via SMAP SCA-V. The SMAP Level-3 Enhanced data spans from March 31, 2015, through to the present day.

To assess SMAP *SM* at the Tambopata, Manaus, and Caxiuana sites, a comparative analysis was conducted between SMAP *SM* data and in situ *SM* observations. Since in situ observations are at a point scale, SMAP Level-3 Enhanced data, which have the finest grid size (9 km) and quality controlled among SMAP *SM* products, was utilized. Hereinafter, SMAP *SM* refers to SMAP Level-3 Enhanced *SM* product. The SMAP *SM* data corresponding to each site was extracted from the 9-km EASE2 grid of the SMAP *SM* by aligning with the center coordinate of the grid cell in closest proximity to the site location (Fig. 1).

C. GPM IMERG Precipitation Product

The Integrated Multi-satellitE Retrievals for Global Precipitation Measurement (IMERG) is an integrated algorithm developed by the U.S. Global Precipitation Measurement (GPM) team, providing a comprehensive multisatellite-based precipitation dataset. The GPM Level-3 IMERG daily 10 km product (hereafter, GPM IMERG), (GPM_3IMERGDF, version 6 [45]) from the NASA Goddard Earth Sciences Data and Information Services Center is used in this study. IMERG aggregates daily precipitation retrievals from June 1, 2000 to September 30, 2021. In alignment with the extraction process of SMAP data, the GPM IMERG data for the study sites is also retrieved according to the grid cell covering individual sites.

D. SMAP SM Retrieval Algorithm

The SMAP *SM* retrieval algorithm uses microwave radiometry to estimate *SM* by parameterizing the L-band T_B model for the canopy and soil. The SMAP provides three different *SM* estimates obtained from the SCA-V, SCA-H, and DCA algorithms. Both SCA-V and SCA-H employ T_{BV} and T_{BH}, respectively, while DCA utilizes both T_B observations. These differing polarizations result in distinct characteristics in the T_B observations. Specifically, the electric field vector of the T_{BV} is oriented perpendicular to the Earth's surface, rendering it less susceptible to surface roughness. Conversely, in T_{BH} measurements, the electric field vector is aligned parallel to the Earth's surface, making these measurements more sensitive to variations in surface roughness. The response of the T_{BV} measurement of geophysical changes in the scene is more stable than that of the T_{BH} [46], [47], and SCA-V *SM* retrieval performs better than SCA-H [44], [48]. In this study, we employed SCA-V, a forward model using T_{BV} only. The canopy effect of the SMAP SCA approach is based on the $\tau-\omega$ model, a simplified representation of the radiative transfer equation for the soil-canopy system [49]

$$T_B^{sim} = T_s\, e\gamma + T_c\,(1-\omega)\,(1-\gamma)\,(1+r\gamma) \tag{1}$$

$$\gamma = exp\,(-\tau sec\theta) \tag{2}$$

where T_B^{sim} is simulated brightness temperature (T_{BV}^{sim} in SCA-V), e is soil emissivity, T_s is the effective soil temperature, T_c is the effective canopy temperature, τ is the *VOD*, ω is the canopy single scattering albedo, r is the soil reflectivity, θ is the SMAP satellite incidence angle (40°), and γ is the transmissivity of the canopy layer. Fig. 2 shows the concept of the $\tau-\omega$ model.

Equations (1) and (2) are used to obtain soil emissivity *e* using SMAP T_B observations and ancillary data of T_s, T_c, and τ. τ is estimated from the ancillary *VWC* as follows:

$$\tau = b \times VWC \tag{3}$$

where *b* is a vegetation type and microwave frequency dependent coefficient obtained from a look-up table. *VWC* is estimated from the NDVI data using land cover-based equations [43].

The SMAP SCA retrieves *SM* through the soil dielectric mixing model. The dielectric constant is resolved from the smooth surface emissivity and the Fresnel equations. The rough surface emissivity is computed from the smooth surface emissivity using a roughness correction parameter *h*. The rough surface emissivity is retrieved from the top-of-the-vegetation T_B using the $\tau-\omega$ model in (1). The current SMAP SCA implementation uses the Mironov soil dielectric model [50], also known as the mineralogy-based soil dielectric model. Mironov's model uses parameters from a large soil database, including frequency of radiometer, observed *SM*, and clay fraction. The SMAP SCA-V uses observed and simulated T_{BV} (T_{BV}^{obs} and T_{BV}^{sim}) to retrieve *SM* by minimizing the cost function

$$f\ (SM) = \left(T_B^{sim}\,(SM) - T_B^{obs}\right)^2 \tag{4}$$

where T_B^{sim} is the brightness temperature simulated in (1) and T_B^{obs} is the SMAP brightness temperature observations.

E. Variability of Precipitation and SM

Mutual interaction between *SM* and precipitation through various physical mechanisms has been highlighted in prior research [1], [51], [52], [53], [54]. These studies support that *SM* can exert influence on precipitation by affecting evaporation and other surface energy fluxes. Specifically, wetter soil can contribute to higher atmospheric humidity, which in turn leads to increased precipitation. In addition, the increase in surface albedo resulting from wetter soil can promote moisture convergence, which in turn, contributes to enhanced precipitation. Recently, the remote sensing of *SM* through SMAP has enabled the demonstration of correlations between *SM* and precipitation on a global scale. Observations on a global scale reveal a spectrum of correlations that range from strong to weak positive relationships. However, in certain regions, the correlation is observed to range from weak to negative, which can be attributed to the characteristics of the land cover type and the local climatic conditions [53].

To investigate the sensitivity of SMAP *SM* to seasonal variations in rainfall within the Amazon rainforest, seasonal averages were compared, specifically focusing on the rainy season (December to February, DJF) and the dry season (June to August, JJA), as well as the difference between these averages (DJF − JJA). Monthly precipitation data was obtained from the Global Precipitation Climatology Centre, averaged for the period from 2015 to 2019, and presented at a 0.25° grid resolution. This analysis aimed to deepen the understanding of the sensitivity of SMAP *SM* to variations in precipitation across different seasons in the Amazon rainforest.

F. Sensitivity Test and Parameter Optimization Approach

The purpose of the parameter sensitivity test is to explore the changes in the SCA *SM* retrieval algorithm to shifts in vegetation parameters and to assess whether these parameters can be optimized specifically for the Amazon rainforest. SCA *SM* retrieval algorithm for optimization does not include SCA-H, due to its recognized similarity to SCA-V, coupled with its relatively inferior performance. Vegetation parameters τ and ω from the SCA-V algorithm were selected to assess the retrieval

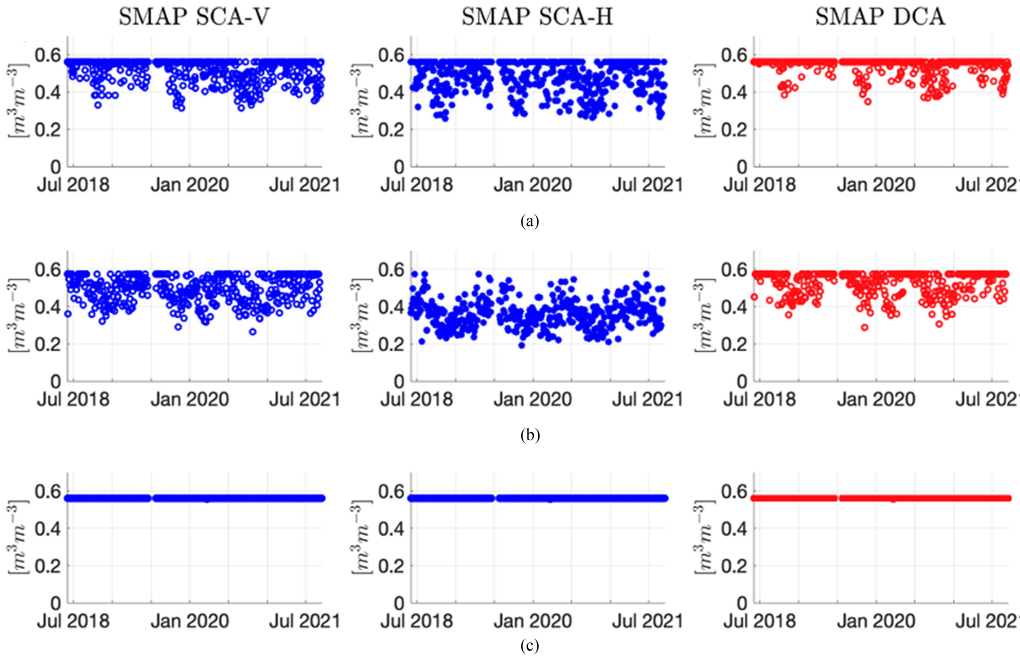

Fig. 3. Time series of SMAP SM retrieved by SMAP SCA with vertically polarized (SCA-V, left column), horizontally polarized (SCA-H, middle column) brightness temperature, and DCA (right column) for the grids covering (a) Tambopata, (b) Manaus, and (c) Caxiuana site. The locations of the sites are shown in Fig. 1.

sensitivity. T_B^{sim} in (4) is strongly influenced not only by T_s and T_c, but also by the ancillary data of τ and ω. In the SMAP SCA-V algorithm, τ is directly proportional to the *VWC* with the coefficient (b) that is contingent on the canopy structure, while ω is a fixed variable based on the land cover type [44]. The ancillary data for SMAP assign a consistent ω of 0.07 across all forest types, and a time-varying τ calculated from (3), for the Amazon rainforest region. Considering the possibility that given SMAP ancillary τ and ω may not accurately represent the dense and tall Amazon rainforest, biases in SMAP *SM* when compared with in situ observations can be expected. To assess the sensitivity of the SMAP *SM* retrievals to τ and ω, a range of values were used. For ω, values within the range of 0.05–0.11, based on the SMAP ancillary data, were used. For τ, the SMAP ancillary value of τ was multiplied by a proportional coefficient ranging from 100% (1×) to 50% (0.5×). The ranges of τ and ω align with those found in the literature [24], [25]. The sensitivity test facilitated the acquisition of optimal τ and ω values for each site. Improvements in the SCA-V *SM* retrievals were assessed using metrics, including Pearson correlation coefficient (r), root mean squared difference (RMSD), mean difference (MEAND), and ubRMSD. Each of these metrics is calculated using (5)–(8), where x represents the model dataset and y represents a reference dataset.

$$RMSD = \sqrt{\frac{1}{N}\sum_{i=1}^{N}(x_i - y_i)^2} \quad (5)$$

$$MEAND = \frac{1}{N}\sum_{i=1}^{N}(x_i - y_i) \quad (6)$$

$$ubRMSD = \sqrt{RMSD^2 - MEAND^2} \quad (7)$$

$$r = \frac{\sum_{i=1}^{N}(x_i - \bar{x})(y_i - \bar{y})}{\sqrt{\sum_{i=1}^{N}(x_i - \bar{x})^2 \sum_{i=1}^{N}(y_i - \bar{y})^2}}. \quad (8)$$

III. Results

A. SMAP SCA and DCA Retrieved SM

Fig. 3 presents the *SM* time series derived from the SMAP SCA-V, SCA-H, and DCA algorithms for three study sites from May 28, 2018 to September 13, 2021. Regardless of the season, SMAP *SM* for all sites and algorithms frequently reaches saturation (*SM* $>$ 0.6 m^3m^{-3}), with this trend being especially pronounced at Tambopata and Caxiuana. At the Manaus site, SMAP *SM* values from SCA-V and DCA remain high (*SM* $>$ 0.35 m^3m^{-3}) and demonstrate minimal seasonal fluctuation (around 0.15 m^3m^{-3}). When comparing SCA-V and SCA-H, the latter shows stronger seasonality and lower values. The Caxiuana site exhibits consistently flat and saturated SM, indicating a decline in SMAP algorithm performance under the dense canopy of the Amazon forest. All three algorithms – SCA-V, SCA-H, and DCA – demonstrate similar seasonal *SM* trends. However, DCA tends to overestimate *SM* more and shows less variation compared with SCA-V and SCA-H.

B. SMAP Soil Moisture and Rainfall

Fig. 4 shows a seasonal variation in SMAP *SM* and rainfall across the Amazon. The SMAP *SM* values during both the wet (DJF) and dry (JJA) seasons display low variability (the maximum difference being less than 0.05 m^3m^{-3}). In contrast, precipitation exhibits a stark distinction between the dry and wet seasons. During the wet season (DJF), precipitation across the

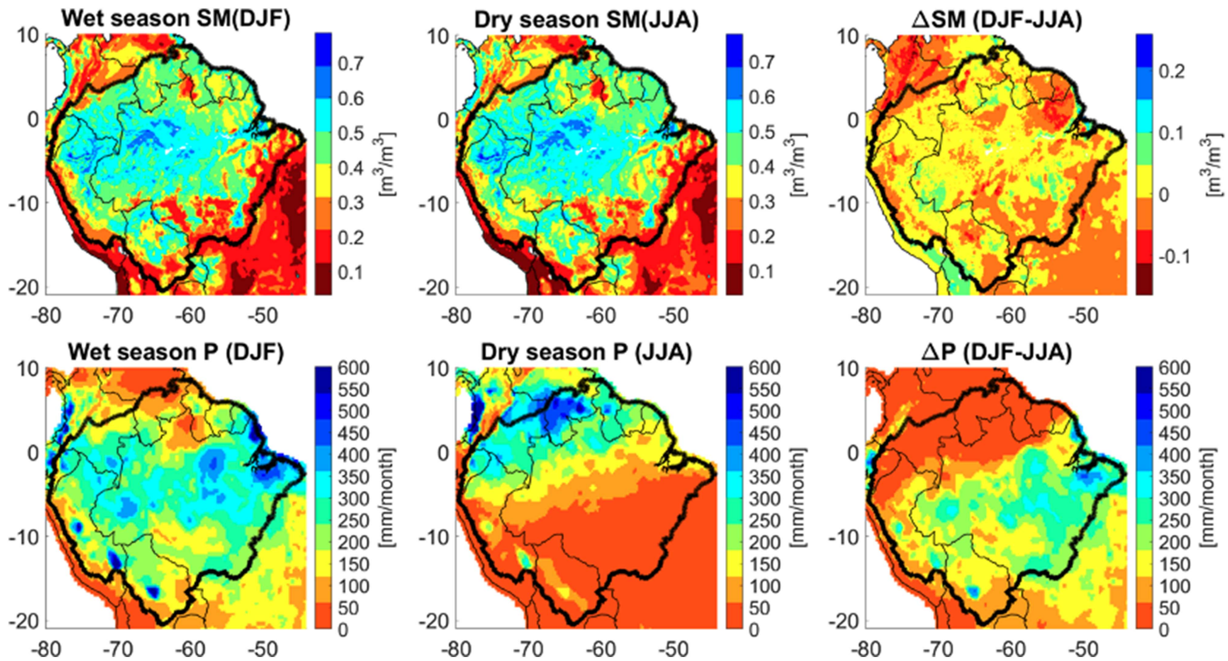

Fig. 4. Seasonal variation of SMAP SM and precipitation(P) over the Amazon rainforest region. From the top left, SM and P of the wet season (December to February, DJF), dry season (June to August, JJA), and the difference between the wet and dry seasons.

TABLE II
CORRELATION COEFFICIENTS BETWEEN DAILY SMAP SCA-V SM AND PRECIPITATION (P) OBSERVATIONS (IN SITU AND IMERG) AT TAMBOPATA, MANAUS, AND CAXIUANA SITES

Site	*In situ* precipitation (point data)	GPM IMERG precipitation (10km gridded data)
Tambopata	0.04	0.07
Manaus	−0.05	0.04
Caxiuana	0	0.02

entire Amazon rainforest region exceeds 150 mm per month, barring the northern parts. Conversely, during the dry season (JJA), precipitation drops below 100 mm per month across most of the southern Amazon. Thus, the SMAP SCA-V *SM* retrievals for the Amazon rainforest do not follow the seasonal shifts in precipitation.

Table II displays the correlation coefficients between daily SMAP SCA *SM* and precipitation data, both in situ (point) and from IMERG (~10 km grid). Since precipitation significantly influences seasonal variations in *SM*, a notable correlation between these variables is expected. However, the observed correlation with both in situ and IMERG remotely sensed precipitation data is low (r < 0.1). This low correlation implies that the SMAP SCA-V *SM* retrieval may not adequately capture the seasonal *SM* variation in the Amazon rainforest.

C. Brightness Temperature and Effective Temperature

In addition to T_B, the effective temperature of soil and vegetation are essential inputs for SMAP *SM* retrievals, as indicated in (1). Fig. 5 compares SMAP ancillary data of modeled effective surface temperature and SMAP T_B observations with corresponding in situ observations. The magnitude and seasonal trend of the SMAP ancillary surface temperature align well with in situ observations, but the latter display larger fluctuations. Moreover, the T_{BV} and T_{BH} exhibit a similar trend, with minor differences in magnitude. These differences can provide insights into the extent of vegetation attenuation. DCA uses the difference to simulate *SM* and τ. Consequently, polarized T_B exhibiting similar trends and magnitudes are generally considered to lack significant informational content.

D. Comparison of SMAP SM to In Situ SM

Fig. 6 compares SMAP *SM* data with in situ *SM* observations at various depths and times. Considering in situ *SM* measured at limited depths, the comparison analysis focuses on the correlation coefficient to characterize temporal variations of SM. At Tambopata [Fig. 6(a)], a single depth *SM* at 5 cm in situ observation is available. Significant differences in magnitude ($> 0.2\ m^3m^{-3}$) are evident with a correlation coefficient r > 0.6. Both SMAP SCA-V and SCA-H *SM* are overestimated compared with in situ observations. Fig. 6(b) compares SMAP *SM* with in situ observations at different depths (2.5 cm) at the Manaus site. In situ *SM* observations at 2.5 cm depth align with SMAP *SM* in terms of relative magnitude compared to that for the Tambopata site. The correlation coefficient between SMAP *SM* and in situ *SM* is lower (r < 0.3). Note that most SMAP SCA-V data points remain at saturation and SMAP SCA-H *SM* is under-estimated compared with in situ *SM*. Fig. 6(c) contrasts SMAP *SM* with in situ observations at the 20 cm depth at Caxiuana, the shallowest measurement depth available. In situ observations at Caxiuana over a longer period show strong seasonality with a dry season from August to December, yet SMAP *SM* does not capture this in situ *SM* seasonality at Caxiuana (r = 0). Both SMAP SCA-V and SCA-H *SM* show

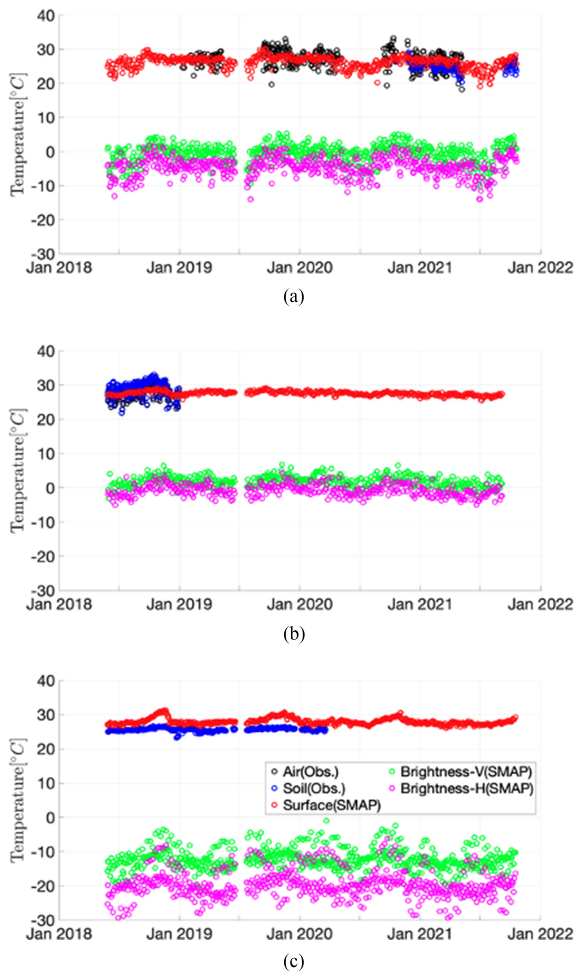

Fig. 5. Time series of in situ observations (Obs.) and SMAP measured (SMAP) temperatures including surface temperature (Surface), T_BV(Brightness-V), and T_BH(Brightness-H) for sites (a) Tambopata, (b) Manaus, and (c) Caxiuana. The in situ observations of air and soil surface temperatures are employed as a reference of effective temperature inputs for the SCA SM retrieval.

saturation for the whole period. The findings suggest that the performance of the SMAP retrieval algorithms is site dependent as reflected in the ancillary data.

The SMAP *SM* retrievals across the Amazon sites display site-specific performance variations. The SCA-V *SM* generally tends to be over-estimated with lower sensitivity to T_B. In contrast, the performance of SCA-H *SM* is more variable as expected since horizontal polarization is less responsive to the vertical structures on the surface.

E. Comparison of GPM IMERG and In Situ Precipitation

To understand the effect of the spatial resolution ($\sim$ 10 km) of satellite remote sensing data on the (low) variation of the SMAP *SM* retrievals, we conducted a comparison analysis of satellite-derived and in situ measurements of precipitation using the GPM IMERG precipitation of the same resolution ($\sim$ 10 km) as that of the SMAP *SM* data. Fig. 7 illustrates the comparison of GPM IMERG and in situ precipitation data for each site. The correlation between in situ and remotely sensed precipitation (Manaus: r = 0.54, Caxiuana: r = 0.64) is higher than that of the

TABLE III
COMPARISON OF OPTIMIZED SMAP SCA-V ALGORITHM RESULTS WITH IN SITU OBSERVATIONS FOR SM AT TAMBOPATA, MANAUS, AND CAXIUANA SITES

Site	Case	Parameter		r	RMSD (m^3m^{-3})	MEAND (m^3m^{-3})	ubRMSD (m^3m^{-3})
		τ	ω				
Tambopata	Default	τ	0.07	0.61	0.30	0.30	0.06
	Optimized	τ*0.9	0.10	0.60	0.05	~0	0.05
Manaus	Default	τ	0.07	0.20	0.11	0.07	0.07
	Optimized	τ*0.9	0.07	0.21	0.07	<0.01	0.07
Caxiuana	Default	τ	0.07	0	0.23	0.22	0.06
	Optimized	τ*0.5	0.11	0.07	0.07	<0.01	0.07

SM observation comparisons (r $<$ 0.4). Given that precipitation strongly influences seasonal variations of *SM*, these findings suggest that the low correlation between different *SM* data is not caused by the resolution discrepancy between point-based and grid-based measurements.

F. Optimization of SM Retrieval

Fig. 8 illustrates a sensitivity test on the SCA-V algorithm at each site using a single depth *SM* measurement (Tambopata: 5 cm, Manaus: 2.5 cm, and Caxiuana: 20 cm). The left panels depict the retrieved *SM* for various τ values, and the right panels show the retrieved *SM* using SCA-V with different ω values. The magnitude and variability of the retrieved *SM* increase in correspondence with τ. The optimal τ value was identified to be 50% lower in Tambopata, 10%–20% lower in Manaus, and 50% lower in Caxiuana than the default values in the SMAP ancillary data. The average τ value decreased from 1.24 to 0.62 in Tambopata, from 1.23 to 1.04 in Manaus, and from 1.24 to 0.62 in Caxiuana. This adjustment resulted in the closest alignment between the retrieved *SM* and the in situ observations at each respective site. Conversely, the magnitude of the retrieved *SM* decreases as the ω value increases. The closest agreement between SMAP retrieval and observed *SM* occurs with ω values of 0.10 (Tambopata), 0.08 (Manaus), and larger than 0.10 (Caxiuana) for each site.

Optimized *SM* retrievals are evaluated using two metrics (RMSD and MEAND). These metrics determine the optimized values of τ and ω for each site. Fig. 9 shows the optimized time series of SCA-V *SM* retrievals for the Tambopata, Manaus, and Caxiuana sites. Minimizing RMSD and MEAND yields similar *SM* retrievals, having a consistent magnitude compared with in situ observations. However, the MEAND-optimized retrievals exhibited more variability than those RMSD-optimized retrievals. Despite this, the optimized parameters do not entirely capture the seasonal and interannual *SM* variability.

Table III displays the default and optimized values of τ and ω corresponding to each evaluation metric. The RMSD-optimized parameters outperform the default parameters, although they show less improvement in ubRMSD. For all three sites (Tambopata, Manaus, and Caxiuana), the optimized τ is smaller (90%, 90%, and 50%) than the ancillary data, while the optimized ω (0.10, 0.07, and 0.11) is similar or higher than the ancillary data value (0.07), aligning with the sensitivity tests presented in Fig. 8.

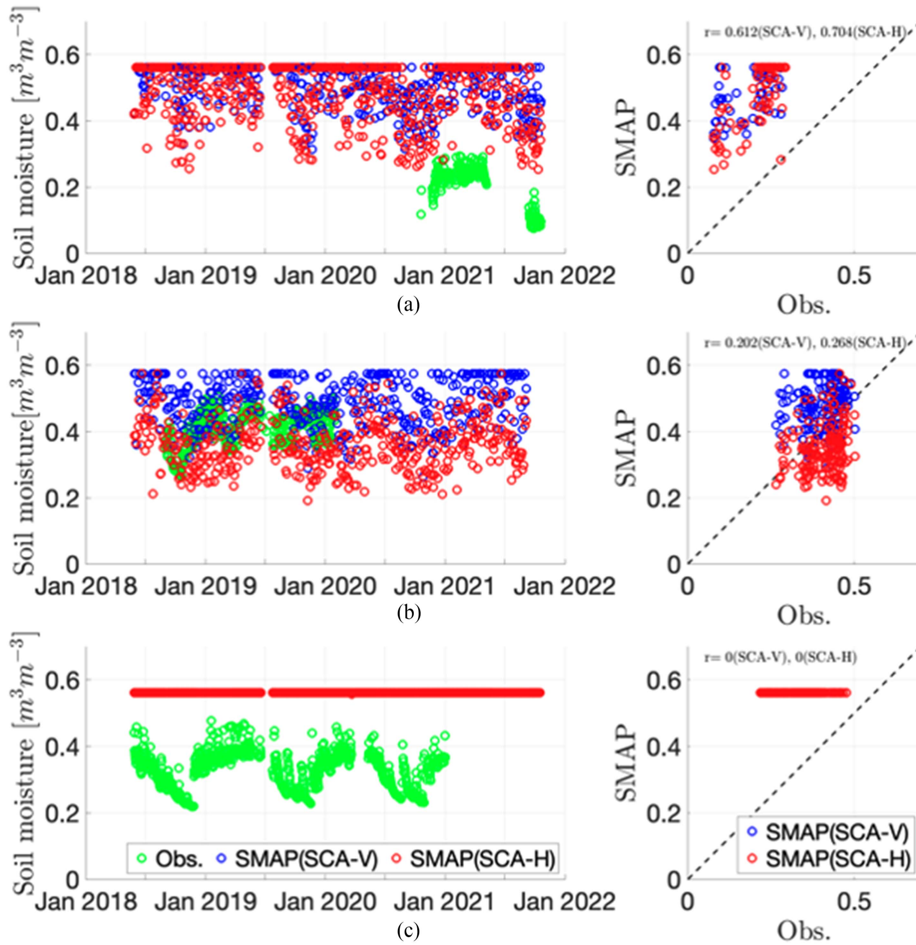

Fig. 6. Comparison between SMAP SM (SCA-V and SCA-H) and *in-situ* measured SM (Obs.). The depth of the SM measurements used for this analysis is (a) 0.05 m at the Tambopata site, (b) 0.025 m at the Manaus site, and (c) 0.2 m at the Caxiuana site, representing the shallowest layer of measurement for each location.

VI. Discussion

We observed significant differences between the SMAP Level-3 Enhanced *SM* product and the in situ observations in the Amazon rainforest. Assessing the SMAP *SM* products against in situ observations in the Amazon rainforest can contribute to the improvement of the SMAP *SM* algorithm and enhance our understanding of climate change and the impacts of extreme climate events in the Amazon rainforest and similar tropical ecosystems.

Previous literature has successfully validated SMAP *SM* using in situ observations across various land cover types [13], [17], [18], [19], [44], [48], [55]. These studies have demonstrated the robust performance of the SMAP algorithms with a low ubRMSD of less than 0.04 m^3m^{-3}. However, an evident knowledge gap exists pertaining to the validation of SMAP *SM* products in tropical rainforests, such as the Amazon rainforest, which are characterized by dense vegetation and tall trees. We anticipate that the quality of SMAP *SM* data for other tropical forest regions would be comparable to the findings in our analysis conducted in the Amazon rainforest.

Our analysis identified two dominant factors contributing to the biases between the SMAP *SM* and in situ observations. First, the coarse spatial resolution of the SMAP *SM* data, with a grid spacing of 9 km and a radiometric resolution of 33 km, may hinder the accurate representation of the complex Amazon landscape and create a significant resolution gap compared with the point scale in situ observations. Second, the dense and tall canopy layer of the Amazon rainforest can affect passive radiometer measurements by attenuating microwave radiation more strongly [56], [57], [58].

For instance, at the Caxiuana site, the SMAP *SM* consistently exhibits saturation levels around 0.6, contrasting with the observed seasonal fluctuations in the in situ *SM* observations (Fig. 6). This saturation is likely due to the presence of surrounding Amazon lakes and reservoirs within the grid area (static water fraction is 15% based on the SMAP ancillary data) and the dense vegetation with an average tree height of 35 m. The comparison of SMAP *SM* with SMAP brightness temperature, in situ observations, and precipitation data (Fig. 4, Table I) highlights the inadequacy of the SMAP *SM* in capturing the seasonal variability in *SM* and its response to precipitation, not only in Caxiuana but also across the broader Amazon rainforest.

Our analysis suggests that the current SMAP SCA-V retrieval algorithm underestimates the vegetation transmissivity

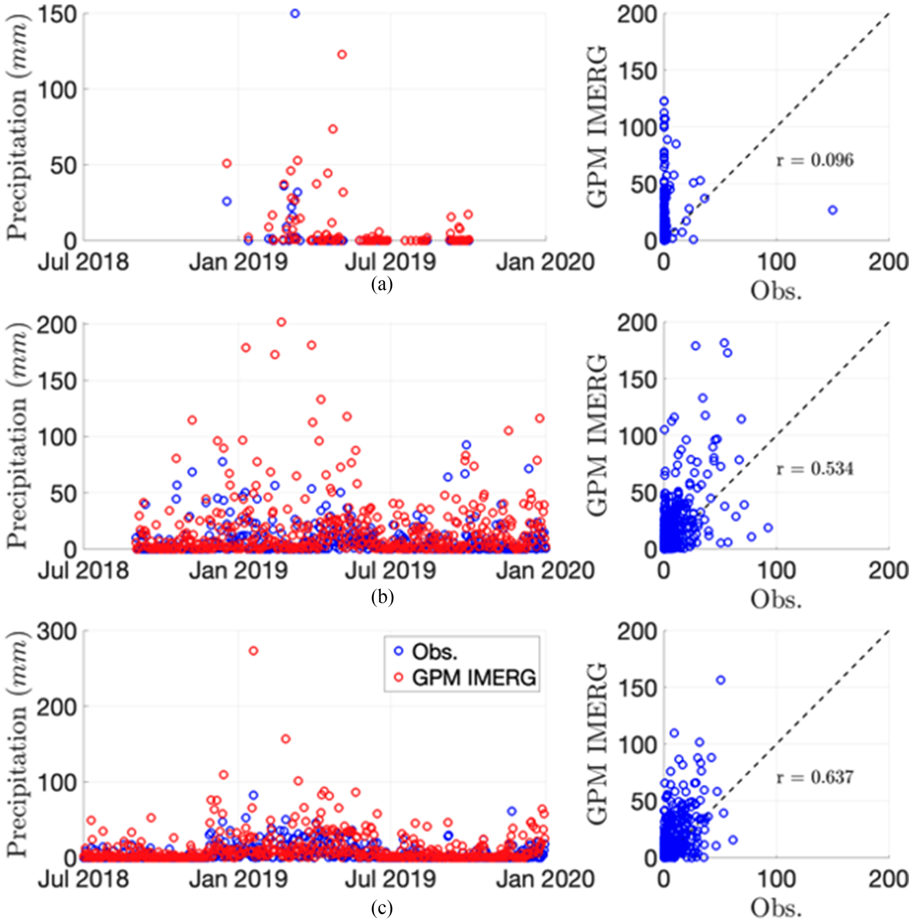

Fig. 7. Comparison between GPM IMERG and *in-situ* measured precipitation (Obs.). The GPM IMERG dataset has a spatial resolution of a 10 km grid. For each site location – (a) Tambopata site, (b) Manaus site, and (c) Caxiuana site – data from GPM IMERG is extracted based on the grid coverage corresponding to these specific locations.

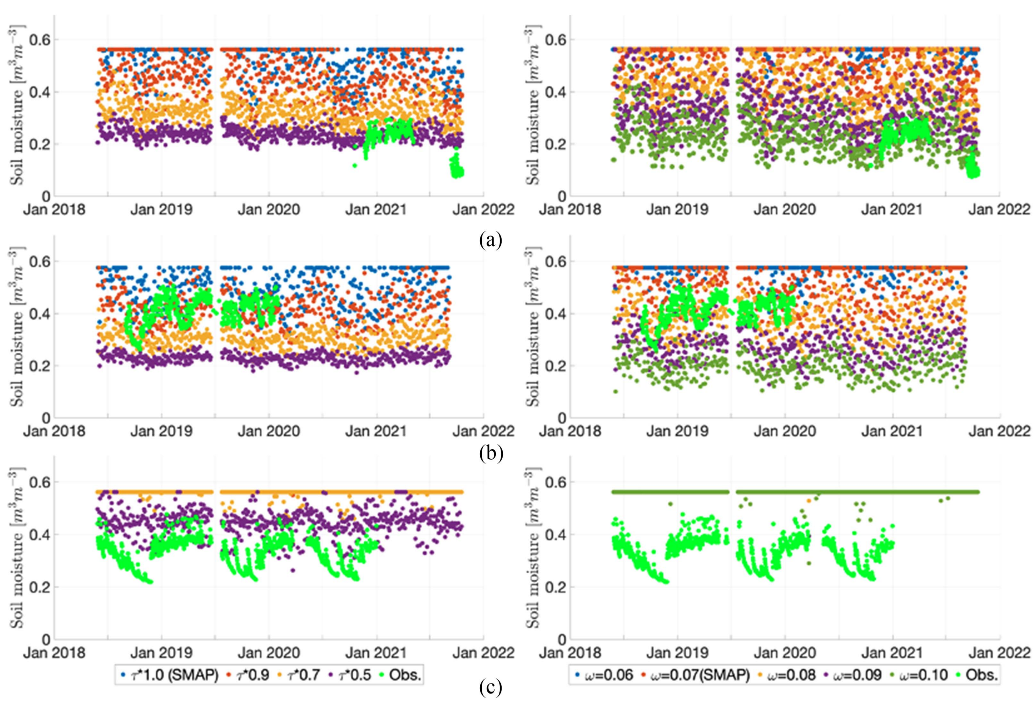

Fig. 8. Sensitivity test result of two $\tau-\omega$ model parameters (τ: left column, ω: right column) to the SM retrieval at (a) Tambopata, (b) Manaus, and (c) Caxiuana sites.

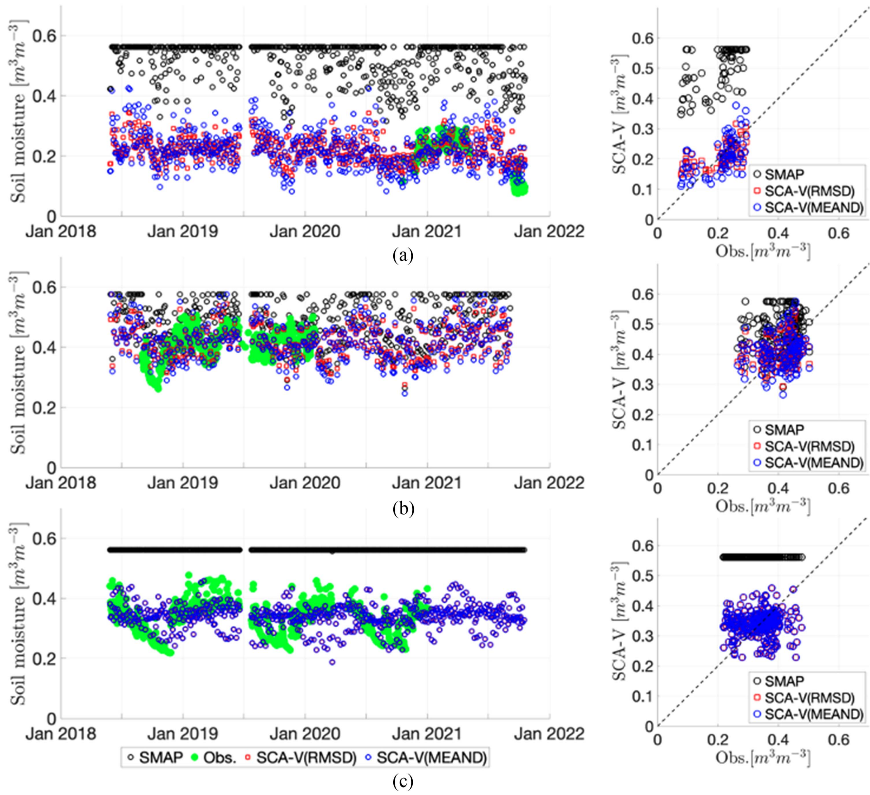

Fig. 9. SM retrieval at (a) Tambopata, (b) Manaus, and (c) Caxiuana sites using optimized SCA-V algorithm for different evaluation metrics (RMSD and MEAND).

of a dense canopy, affecting the *SM* retrieval. While SMAP algorithms perform well for the temperate forest areas [19], they face challenges for tropical forest regions such as the Amazon where the canopy is much denser and thicker. By optimizing vegetation-related SCA-V parameters, namely τ and ω, we observed improvements in the *SM* retrieval from SMAP data. Lowering τ by 10% in Tambopata, 10% in Manaus, and 50% in Caxiuana altered both the magnitude and variability of *SM*, while adjusting ω by 43% in Tambopata, and 57% in Caxiuana fine-tuned the magnitude of *SM*. However, it is crucial to note that these adjustments have limitations, and optimizing τ and ω alone may not be sufficient to universally improve the SMAP *SM* retrieval algorithm, as optimal parameters may vary across the Amazon rainforest.

Through the optimization of τ and ω, we also found that the low transmissivity of the Amazon rainforest due to the dense and thick canopy layer with high *VWC* results in lower T_B^{sim}. To make T_B^{sim} closer to the T_B^{obs}in (4), the SMAP algorithm retrieves higher *SM* to increase surface emissivity in response to the low transmissivity [in (1)]. An increase in surface emissivity corresponds to an increase in *SM* and T_B^{sim}. This tendency can be observed in the comparison between SMAP T_B^{obs} and SMAP *SM*. The greater variations of T_B (Fig. 5) at Tambopata and Caxiuana than those at the Manaus site were presumably due to greater variability of in situ *SM*. Yet, the variations of SMAP *SM* are greater at Manaus than at Tambopata and Caxiuana (Fig. 3), indicating how overestimated *VWC* in SMAP *SM* diminishes the variation of SMAP T_B^{obs}. Similarly, the comparison of SMAP *SM* with in situ observations and precipitation data (Figs. 4, 6, and 7) highlights the insufficiency of the SMAP baseline *SM* retrieval algorithm in capturing *SM* beneath the dense canopy layer. The results from the Caxiuana site demonstrate that the information in SMAP brightness temperature might be interpreted as either a lack of signal detection beneath the vegetation cover or as detecting the vegetation cover itself. This study has shown that through parameter optimization, it is possible to retrieve variations of surface *SM* even under dense vegetation cover. This underscores the need for further refinement of the algorithm and the potential integration of in situ data to enhance the accuracy of *SM* estimations in regions characterized by dense forest cover.

The presumption is that L-band radiation, with a frequency of 1.41 GHz, can penetrate the leaves within forest canopies. However, the structure of the canopy, including elements such as trunks, branches, and stems, influences the microwave emissions emanating from the soil and canopy, which consequently diminishes the transmissivity [59]. Moreover, the dense canopies of tropical rainforests typically hold higher quantities of water in their stems during the dry seasons, which is essential for transpiration [36], [60]. As such, it is imperative for future research to incorporate additional parameters beyond τ and ω in the forward modeling of T_B, including considerations, such as the vegetation type, structural characteristics, and water dynamics. In addition to other factors, a significant static water fraction can skew the T_B readings of a grid cell, which may lead to inaccurate *SM* representations, contributing to the minimal variation observed at the Caxiuana site. While the SMAP *SM* retrieval algorithm currently does adjust for water body emissivity, the correction uses a static water body mask. Including a consideration for changing water body area, alongside enhancements for vegetation characteristics, could lead to more accurate *SM* estimations in regions like the Amazon rainforest, where water bodies are varied and widespread. This enhancement would facilitate more precise retrievals of *SM* using SMAP data, contributing to the accuracy and utility of remote sensing in hydrological and environmental studies.

However, it is important to acknowledge the limitations of this study, including the limited depth and number of in situ observations and the scale gap between the in situ and SMAP data. The in situ *SM* observations at depths deeper than 5 cm challenge the comparison with SMAP *SM*, leading to inconsistencies in the overall evaluation. However, the available data demonstrate consistent seasonal trends in *SM* across different depths, suggesting that our observations can reliably represent the seasonal *SM* variation for each location in the study. The limited in situ observation points (one point per each site in this study) and associated their time series make it difficult to analyze the interannual variability of *SM*. Even though this analysis uses single point-scale in situ *SM* observations at each site, the biases of the SMAP *SM* retrievals are arguably representative of the Amazon region since the SMAP *SM* have substantial biases at all Amazon sites with in situ observations. Colliander et al. [17] highlighted the need for spatially distributed observations from multiple sensors to accurately represent *SM* at a 9 km resolution. Single-point observations may be biased compared with the area average and may not represent the spatial distribution of *SM* over the study domain. Therefore, it is desirable to use multiple sensors to validate and further improve the *SM* retrievals. Despite the inherent limitations associated with analyses based on single-point in situ observations, our study suggests that the temporal variations of *SM* at a single point offer valuable insights into the temporal variations of SMAP *SM*, thereby enhancing the understanding of remotely sensed *SM* dynamics [17].

V. Conclusion

This study is the first assessment of the SMAP *SM* for the Amazon rainforest using in situ observations. Comparison between the current SMAP *SM* and in situ observations showed substantial differences in all three study areas. Our findings suggest that *SM* retrieval algorithms need to improve for tropical rainforest areas with dense and tall vegetation. The current SMAP SCA-V algorithm overestimates *SM* for the Amazon region due to high *VWC*.

Improvement of the SMAP *SM* retrievals for the Amazon rainforest region may be achieved by optimizing two key parameters of the SCA-V algorithm, τ and ω. Lowering the value of the SMAP default τ can significantly reduce biases of the SCA-V *SM* retrievals to be consistent with in situ observations. In densely vegetated areas, overestimated τ makes the SMAP SCA algorithm retrieve *SM* higher as an offset for the high τ within the algorithm. It is important to ensure that τ and ω are adjusted within reasonable ranges.

For more accurate SMAP *SM* retrieval in the Amazon rainforest region, considering additional canopy-related parameters is crucial. This includes factors like vegetation type, structure, and water dynamics, impacting the estimation of *VWC*. Although optimizing τ and ω parameters significantly reduces bias, this approach is constrained due to the limited availability of in situ *SM* observations. To enhance the SMAP *SM* retrievals across the entirety of the Amazon region, a novel approach not relying on in situ observations is needed.

References

[1] R. D. Koster et al., "Regions of strong coupling between soil moisture and precipitation," *Science*, vol. 305, no. 5687, pp. 1138–1140, 2004.

[2] R. D. Koster et al., "GLACE: The global land–atmosphere coupling experiment. Part I: Overview," *J. Hydrometeorol.*, vol. 7, no. 4, pp. 590–610, 2006.

[3] J. Sheffield and E. F. Wood, "Global trends and variability in soil moisture and drought characteristics, 1950–2000, from observation-driven simulations of the terrestrial hydrologic cycle," *J. Climate*, vol. 21, no. 3, pp. 432–458, 2008.

[4] K. Das and P. K. Paul, "Present status of soil moisture estimation by microwave remote sensing," *Cogent Geosci.*, vol. 1, no. 1, 2015, Art. no. 1084669.

[5] S. E. Tuttle and G. D. Salvucci, "A new approach for validating satellite estimates of soil moisture using large-scale precipitation: Comparing AMSR-E products," *Remote Sens. Environ.*, vol. 142, pp. 207–222, 2014.

[6] D. B. Metcalfe et al., "The effects of water availability on root growth and morphology in an Amazon rainforest," *Plant Soil*, vol. 311, pp. 189–199, 2008.

[7] D. Markewitz, S. Devine, E. A. Davidson, P. Brando, and D. C. Nepstad, "Soil moisture depletion under simulated drought in the Amazon: Impacts on deep root uptake," *New Phytologist*, vol. 187, no. 3, pp. 592–607, 2010.

[8] Y. Pokhrel et al., "Global terrestrial water storage and drought severity under climate change," *Nature Climate Change*, vol. 11, no. 3, pp. 226–233, 2021.

[9] L. Meng et al., "Soil moisture thresholds explain a shift from light-limited to water-limited sap velocity in the Central Amazon during the 2015–16 El Niño drought," *Environ. Res. Lett.*, vol. 17, no. 6, 2022, Art. no. 064023.

[10] E. T. Engman, "Applications of microwave remote sensing of soil moisture for water resources and agriculture," *Remote Sens. Environ.*, vol. 35, no. 2-3, pp. 213–226, 1991.

[11] E. Babaeian, M. Sadeghi, S. B. Jones, C. Montzka, H. Vereecken, and M. Tuller, "Ground, proximal, and satellite remote sensing of soil moisture," *Rev. Geophys.*, vol. 57, no. 2, pp. 530–616, 2019.

[12] D. Entekhabi et al., "The soil moisture active passive (SMAP) mission," *Proc. IEEE*, vol. 98, no. 5, pp. 704–716, May 2010.

[13] R. Zhang, S. Kim, and A. Sharma, "A comprehensive validation of the SMAP Enhanced Level-3 soil moisture product using ground measurements over varied climates and landscapes," *Remote Sens. Environ.*, vol. 223, pp. 82–94, 2019.

[14] J.-P. Wigneron et al., "Modelling the passive microwave signature from land surfaces: A review of recent results and application to the L-band SMOS & SMAP soil moisture retrieval algorithms," *Remote Sens. Environ.*, vol. 192, pp. 238–262, 2017.

[15] G. P. Petropoulos, G. Ireland, and B. Barrett, "Surface soil moisture retrievals from remote sensing: Current status, products & future trends," *Phys. Chem. Earth, Parts A/B/C*, vol. 83, pp. 36–56, 2015.

[16] P. O'Neill et al., "Evaluation of the validated soil moisture product from the SMAP radiometer," in *Proc. IEEE Int. Geosci. Remote Sens. Symp.*, 2016, pp. 125–128.

[17] A. Colliander et al., "Validation of soil moisture data products from the NASA SMAP mission," *IEEE J. Sel. Topics Appl. Earth Observ. Remote Sens.*, vol. 15, pp. 364–392, 2021.

[18] E. Ayres, A. Colliander, M. H. Cosh, J. A. Roberti, S. Simkin, and M. A. Genazzio, "Validation of SMAP soil moisture at terrestrial national ecological observatory network (NEON) sites show potential for soil moisture retrieval in forested areas," *IEEE J. Sel. Topics Appl. Earth Observ. Remote Sens.*, vol. 14, pp. 10903–10918, 2021.

[19] A. Colliander et al., "SMAP detects soil moisture under temperate forest canopies," *Geophysical Res. Lett.*, vol. 47, no. 19, 2020, Art. no. e2020GL089697.

[20] J. T. Ambadan et al., "Evaluation of SMAP soil moisture retrieval accuracy over a boreal forest region," *IEEE Trans. Geosci. Remote Sens.*, vol. 60, 2022, Art. no. 4414611.

[21] T. W. Crowther et al., "Mapping tree density at a global scale," *Nature*, vol. 525, no. 7568, pp. 201–205, 2015.

[22] P. Potapov et al., "Mapping global forest canopy height through integration of GEDI and Landsat data," *Remote Sens. Environ.*, vol. 253, 2021, Art. no. 112165.

[23] S. Chan, R. Bindlish, R. Hunt, T. Jackson, and J. Kimball, "Vegetation water content," Jet Propulsion Laboratory, California Institute of Technology, Pasadena, CA, USA, 2013.

[24] A. G. Konings, M. Piles, N. Das, and D. Entekhabi, "L-band vegetation optical depth and effective scattering albedo estimation from SMAP," *Remote Sens. Environ.*, vol. 198, pp. 460–470, 2017.

[25] M. J. Chaubell et al., "Improved SMAP dual-channel algorithm for the retrieval of soil moisture," *IEEE Trans. Geosci. Remote Sens.*, vol. 58, no. 6, pp. 3894–3905, Jun. 2020.

[26] J. Chaubell et al., "Regularized dual-channel algorithm for the retrieval of soil moisture and vegetation optical depth from SMAP measurements," *IEEE J. Sel. Topics Appl. Earth Observ. Remote Sens.*, vol. 15, pp. 102–114, 2021.

[27] X. Li et al., "A new SMAP soil moisture and vegetation optical depth product (SMAP-IB): Algorithm, assessment and inter-comparison," *Remote Sens. Environ.*, vol. 271, 2022, Art. no. 112921.

[28] T. Zhao et al., "Retrievals of soil moisture and vegetation optical depth using a multi-channel collaborative algorithm," *Remote Sens. Environ.*, vol. 257, 2021, Art. no. 112321.

[29] A. F. Feldman, D. Chaparro, and D. Entekhabi, "Error propagation in microwave soil moisture and vegetation optical depth retrievals," *IEEE J. Sel. Topics Appl. Earth Observ. Remote Sens.*, vol. 14, pp. 11311–11323, 2021.

[30] A. G. Konings, K. A. McColl, M. Piles, and D. Entekhabi, "How many parameters can be maximally estimated from a set of measurements?," *IEEE Geosci. Remote Sens. Lett.*, vol. 12, no. 5, pp. 1081–1085, May 2015.

[31] A. G. Konings, M. Piles, K. Rötzer, K. A. McColl, S. K. Chan, and D. Entekhabi, "Vegetation optical depth and scattering albedo retrieval using time series of dual-polarized L-band radiometer observations," *Remote Sens. Environ.*, vol. 172, pp. 178–189, 2016.

[32] H. Ma et al., "An assessment of L-band surface soil moisture products from SMOS and SMAP in the tropical areas.," *Remote Sens. Environ.*, vol. 284, 2023, Art. no. 113344.

[33] N. Kunert et al., "A revised hydrological model for the Central Amazon: The importance of emergent canopy trees in the forest water budget," *Agricultural Forest Meteorol.*, vol. 239, pp. 47–57, 2017.

[34] E. Salati, A. Dall'Olio, E. Matsui, and J. R. Gat, "Recycling of water in the Amazon basin: An isotopic study," *Water Resour. Res.*, vol. 15, no. 5, pp. 1250–1258, 1979.

[35] R. D. Bruno, H. R. Da Rocha, H. C. De Freitas, M. L. Goulden, and S. D. Miller, "Soil moisture dynamics in an eastern Amazonian tropical forest," *Hydrological Processes: Int. J.*, vol. 20, no. 12, pp. 2477–2489, 2006.

[36] R. I. N. Juárez, M. G. Hodnett, R. Fu, M. L. Goulden, and C. Von Randow, "Control of dry season evapotranspiration over the Amazonian forest as inferred from observations at a southern Amazon forest site," *J. Climate*, vol. 20, no. 12, pp. 2827–2839, 2007.

[37] R. Negrón-Juárez et al., "Calibration, measurement, and characterization of soil moisture dynamics in a central Amazonian tropical forest," *Vadose Zone J.*, vol. 19, no. 1, 2020, Art. no. e20070.

[38] V. Lakshmi, E. F. Wood, and B. J. Choudhury, "A soil-canopy-atmosphere model for use in satellite microwave remote sensing," *J. Geophysical Res.: Atmospheres*, vol. 102, no. D6, pp. 6911–6927, 1997.

[39] G. Lopez-Gonzalez, M. Burkitt, S. Lewis, and O. Phillips, "ForestPlots.net–managing permanent plot information across the tropics," *Biodiversity Ecol.*, vol. 4, pp. 95–103, 2012.

[40] M. O. Andreae et al., "Biogeochemical cycling of carbon, water, energy, trace gases, and aerosols in Amazonia: The LBA-EUSTACH experiments," *J. Geophysical Res.: Atmospheres*, vol. 107, no. D20, pp. LBA 33–1–LBA 33–25, 2002.

[41] P. E. O'Neill et al., "SMAP enhanced L3 radiometer global and polar grid daily 9 km EASE-grid soil moisture, version 5," NASA National Snow and Ice Data Center Distributed Active Archive Center, Boulder, CO, USA, 2021.

[42] S. K. Chan et al., "Development and assessment of the SMAP enhanced passive soil moisture product," *Remote Sens. Environ.*, vol. 204, pp. 931–941, 2018.

[43] P. B. O'Neill, S. Chan, J. Chaubell, E. Njoku, and T. Jackson, "Soil moisture active passive (SMAP) algorithm theoretical basis document level 2 & 3 soil moisture (passive) data product document," Jet Propulsion Laboratory, California Institute of Technology, No. JPL D-66480 2020, 2020. [Online]. Available: https://smap.jpl.nasa.gov/system/internal_resources/details/original/484_L2_SM_P_ATBD_rev_F_final_Aug2020.pdf

[44] A. Colliander et al., "Validation of SMAP surface soil moisture products with core validation sites," *Remote Sens. Environ.*, vol. 191, pp. 215–231, 2017.

[45] G. J. Huffman, E. F. Stocker, D. T. Bolvin, E. J. Nelkin, and J. Tan, "GPM IMERG final precipitation L3 1 day 0.1 degree x 0.1 degree V06, edited by Andrey Savtchenko, Greenbelt, MD, Goddard Earth Sciences Data and Information Services Center (GES DISC)," 2019. Accessed: Dec. 12, 2023. [Online]. Available: https://doi.org/10.5067/GPM/IMERGDF/DAY/06

[46] T. L. Rowlandson et al., "Capturing agricultural soil freeze/thaw state through remote sensing and ground observations: A soil freeze/thaw validation campaign," *Remote Sens. Environ.*, vol. 211, pp. 59–70, 2018.

[47] N. M. Holtzman et al., "L-band vegetation optical depth as an indicator of plant water potential in a temperate deciduous forest stand," *Biogeosciences*, vol. 18, no. 2, pp. 739–753, 2021.

[48] S. K. Chan et al., "Assessment of the SMAP passive soil moisture product," *IEEE Trans. Geosci. Remote Sens.*, vol. 54, no. 8, pp. 4994–5007, Aug. 2016, doi: 10.1109/tgrs.2016.2561938.

[49] T. Mo, B. J. Choudhury, T. J. Schmugge, J. R. Wang, and T. J. Jackson, "A model for microwave emission from vegetation-covered fields," *J. Geophysical Res.: Oceans*, vol. 87, no. C13, pp. 11229–11237, 1982.

[50] V. L. Mironov, L. G. Kosolapova, and S. V. Fomin, "Physically and mineralogically based spectroscopic dielectric model for moist soils," *IEEE Trans. Geosci. Remote Sens.*, vol. 47, no. 7, pp. 2059–2070, Jul. 2009.

[51] D. Entekhabi, I. Rodriguez-Iturbe, and F. Castelli, "Mutual interaction of soil moisture state and atmospheric processes," *J. Hydrol.*, vol. 184, no. 1-2, pp. 3–17, 1996.

[52] X. Zheng and E. A. Eltahir, "A soil moisture–rainfall feedback mechanism: 2. Numerical experiments," *Water Resour. Res.*, vol. 34, no. 4, pp. 777–785, 1998.

[53] R. Sehler, J. Li, J. Reager, and H. Ye, "Investigating relationship between soil moisture and precipitation globally using remote sensing observations," *J. Contemporary Water Res. Educ.*, vol. 168, no. 1, pp. 106–118, 2019.

[54] N. K. Singh, R. E. Emanuel, B. L. McGlynn, and C. F. Miniat, "Soil moisture responses to rainfall: Implications for runoff generation," *Water Resour. Res.*, vol. 57, no. 9, 2021, Art. no. e2020WR028827.

[55] A. Colliander et al., "Validation and scaling of soil moisture in a semi-arid environment: SMAP validation experiment 2015 (SMAPVEX15)," *Remote Sens. Environ.*, vol. 196, pp. 101–112, 2017.

[56] T. J. Jackson, T. J. Schmugge, and J. R. Wang, "Passive microwave sensing of soil moisture under vegetation canopies," *Water Resour. Res.*, vol. 18, no. 4, pp. 1137–1142, 1982.

[57] D. M. Le Vine and M. A. Karam, "Dependence of attenuation in a vegetation canopy on frequency and plant water content," *IEEE Trans. Geosci. Remote Sens.*, vol. 34, no. 5, pp. 1090–1096, Sep. 1996.

[58] A. F. Feldman, R. Akbar, and D. Entekhabi, "Characterization of higher-order scattering from vegetation with SMAP measurements," *Remote Sens. Environ.*, vol. 219, pp. 324–338, 2018.

[59] A. Rosenqvist and B. Killough, *A Layman's Interpretation Guide to L-Band and C-Band Synthetic Aperture Radar data*. Washington, DC, USA: Committee on Earth Observation Satellites, 2018.

[60] B. Yan et al., "Modelling tree stem-water dynamics over an Amazonian rainforest," *Ecohydrology*, vol. 13, no. 1, 2020, Art. no. e2180.

Kyeungwoo Cho received the B.Sc. and M.Sc. degrees in civil and environmental engineering from Yonsei University, Seoul, South Korea, in 2018 and 2020, respectively. He is currently working toward the Ph.D. degree in water resources and hydrology with the Department of Civil and Environmental Engineering, Georgia Institute of Technology, Atlanta, GA, USA.

His research is primarily focused on the intersections of remote sensing and hydrological modeling.

Robinson Negrón-Juárez received the B.S. degree in physics from the University of San Marcos, Lima, Peru, in 1994, and the M.Sc. and Ph.D. degrees in meteorology from the University of São Paulo, São Paulo, Brazil, in 1999 and 2004, respectively.

He is a Renowned Scientist in the field of Earth and Environmental Sciences, with a specialization in understanding the impacts of natural disturbances on forest ecosystems. He is an Esteemed Member of the Earth and Environmental Sciences Area with the Lawrence Berkeley National Laboratory.

Andreas Colliander (Senior Member, IEEE) received the M.Sc. (Tech.), Lic.Sc. (Tech.), and D.Sc. (Tech.) degrees from Aalto University, Espoo, Finland, in 2002, 2005, and 2007, respectively, all in electrical engineering.

He is currently a Research Scientist with the Jet Propulsion Laboratory, California Institute of Technology, Pasadena, CA, USA. His research interests include the development of microwave remote sensing techniques. He is currently leading the calibration and validation of the geophysical retrievals of NASA's SMAP mission and developing multifrequency retrievals for ice sheets and polar atmosphere.

Eric G. Cosio received the Ph.D. degree in botany from Miami University, Oxford, OH, USA, in 1984.

He is currently a Full Professor with the Department of Science, Pontifical Catholic University of Peru, Lima, Peru. His research encompasses the study of Andean ecosystems, restoration ecology, and biodiversity conservation. He is also involved in studying plant-plant and plant-microbe interactions, with implications for ecosystem restoration and management. His research has been vital in providing insights into the ecological dynamics of tropical regions, which is essential for developing sustainable conservation strategies.

Norma Salinas received the M.Sc. degree in environmental management and development from the Latin American Faculty of Social Sciences, San José, Costa Rica, in 2005, and the D.Phil. degree in geography and environment from the University of Oxford, Oxford, U.K., in 2011.

She is currently a Senior Research Scientist with the Institute for Nature, Earth and Energy (INTE-PUCP) and is a dedicated Faculty Member with the Pontifical Catholic University of Peru (PUCP), Lima, Peru. She is a Distinguished Biologist and Environmental Scientist. She founded the Ecosystem Sciences Laboratory, PUCP, contributing significantly to the institution's research capabilities in ecosystem sciences.

Alessandro de Araujo received the bachelor's degree in nautical science from the Admiral Braz de Aguiar Instruction Center, in 1993, followed by a degree in agronomy from the Federal Rural University of Amazonia, Belém, Brazil, in 1999, the M.Sc. degree in geoenvironmental sciences and the Ph.D. degree in geoenvironmental sciences from Vrije Universiteit Amsterdam, Amsterdam, The Netherlands, in 2004 and 2009, respectively.

He is a highly accomplished scientist with extensive expertise in geosciences and a particular focus on micrometeorology of forest and agricultural ecosystems in the Amazon biome. His research encompasses a wide range of topics including environmental biophysics of primary and secondary forest ecosystems, environmental biophysics of agricultural ecosystems in monocultures and agroforestry systems, mass and energy fluxes at the biosphere-atmosphere interface using the eddy covariance technique, and the utilization of stable carbon isotopes to assist in understanding processes in forest ecosystems.

Jefferey Q. Chambers received the B.S. degree (*Cum Laude*) in biochemistry from California Polytechnic State University, San Luis Obispo, CA, USA, in 1992, and the Ph.D. degree in ecology from the University of California, Santa Barbara, Santa Barbara, CA, USA, in 1998.

He is an esteemed environmental scientist currently holding the position of a Senior Scientist with the Earth and Environmental Sciences Area, Lawrence Berkeley National Laboratory, Berkeley, CA, USA. He is also a Faculty Scientist with the Department of Geography, University of California, Berkeley, Berkeley, CA, USA. He has primarily focused on tropical forest dynamics and its linkage to the global carbon cycle. His work often involves using remote sensing data, field observations, and numerical models to investigate the structure, function, and dynamics of tropical forests. Notably, he leads the Next Generation Ecosystem Experiments (NGEE)–Tropics.

Jingfeng Wang received the B.Sc. degree in theoretical and applied mechanics and the M.Sc. degree in computational fluid mechanics from Peking University, Beijing, China, in 1984 and 1987, respectively, and the Sc.D. degree in hydrometeorology from the Massachusetts Institute of Technology, Cambridge, MA, USA, in 1997.

He is currently an Associate Professor with the Georgia Institute of Technology, Atlanta, GA, USA. His research interests include climatology and meteorology, hydrology, and modeling and computational science. His work is instrumental in advancing knowledge and understanding in these critical interdisciplinary areas.